Atmos. Chem. Phys. Discuss., 10, 21303–21321, 2010
www.atmos-chem-phys-discuss.net/10/21303/2010/
doi:10.5194/acpd-10-21303-2010

Atmospheric Chemistry and Physics Discussions

Scale-by-scale analysis of probability distributions for global MODIS-AQUA cloud properties: how the large scale signature of turbulence may impact statistical analyses of clouds

M. de la Torre Juárez, A. B. Davis, and E. J. Fetzer

Jet Propulsion Laboratory/California Institute of Technology, Pasadena, CA 91109-8099, USA

Received: 21 August 2010 – Accepted: 27 August 2010 – Published: 7 September 2010

Correspondence to: M. de la Torre Juárez (mtj@jpl.nasa.gov)

Published by Copernicus Publications on behalf of the European Geosciences Union.

Abstract

Means, standard deviations and Probability distribution functions (PDFs) of cloud properties from the MODerate resolution Infrared Spectrometer are estimated globally as function of averaging scale, varied from 5 to 500 km. These properties – cloud fraction, droplet effective radius, and liquid water path – all matter for cloud-climate uncertainty quantification and reduction efforts. Analytical expressions are identified that fit best to each observed PDF. Global means and standard deviations are confirmed to change with scale. For the range of scales considered, global means vary only within 3% for cloud fraction, 7% for liquid water path, and 0.2% for cloud particle effective radius. These scale dependences contribute to the uncertainties in their global budgets. Scale dependence for standard deviations is compared to predictions for turbulent systems. While the best analytical PDF fit to each variable differs, *all* PDFs are well described by log-normal PDFs when the mean is normalized by the standard deviation inside each averaging domain. Importantly, log-normal distributions yield significantly better fits to the observations than gaussians at all scales. This suggests a possible approach for both sub-grid and unified stochastic modeling of these variables at all scales. The results also highlight the need to establish an adequate spatial resolution for two-stream radiative studies of cloud-climate interactions.

1 Introduction

Cloud impacts on the energy and water cycles remain an important source of uncertainty in our understanding of climate. This applies to the simplest low-dimensional energy balance models (Budyko, 1969; Sellers, 1969; Pujol, 2003), climate sensitivity analyses (e.g. Roe and Baker, 2007; Hannart et al., 2009), two-scale stochastic models (e.g. Imkeller and v. Storch, 2001), and to complex Global Circulation Models (GCMs) incorporated into the Intergovernmental Panel on Climate Change assessments (Solomon, 2007).

ACPD

10, 21303–21321, 2010

The inherent turbulence of atmospheric flows prevents observations and models from capturing the constantly evolving structure of clouds in the atmosphere. This complexity limits our confidence in predictions of cloud properties and therefore of climate sensitivity. Observed cloud properties have, besides, biases dependent on sensor- (e.g. Boers et al., 2006; Horváth and Davies, 2007; Bennartz, 2007) and cloud-types (de la Torre Juárez et al., 2009) that may be smaller than those resulting from limited sampling of highly variable fields (Schutgens and Roebeling, 2009). Therefore, one approach to understand the radiative impact of clouds on climate is to determine the robust statistical distributions of cloud properties rather than solving exactly for each specific cloud field. Although it is widely recognized that there is no justification for assuming gaussian distributions (Hannart et al., 2009), analyses of atmospheric flows and climate often quantify cloud-climate dynamics and uncertainties by interpreting means, standard deviations and confidence levels in gaussian frameworks (e.g. Roe and Baker, 2007). Identifying more realistic distributions gives more credible depictions of observational results, better subgrid parameterizations, and a more rigorous approach to quantifying cloud and climate modeling uncertainties.

Questions also remain open about climate impacts of processes unfolding at the relatively small scales of the clouds themselves. The spatio-temporal scales at which cloud formation, precipitation, and interactions with aerosols occur are largely unresolved by satellite instruments, yet these phenomena determine large-scale properties of clouds relevant to the atmosphere's radiative balance. The ability to characterize statistically a large range of scales can reveal dynamical interactions across scales, and, possibly, to extrapolate these to the small unresolved ones, thus providing relevant validation data for cloud-process models.

Comparisons of trade cumulus cloud fraction statistics over the tropical Western Atlantic at pixel resolutions from the 15-m to the kilometer scale show significant scale-dependence (e.g. Dey et al., 2008). Similar scale-dependence was found in early data-driven stochastic simulations of cloud fields (Shenk and Salomonson, 1972), in observed Outgoing Long-wave Radiation in high tropical Pacific clouds (Pierrehumbert,

ACPD
10, 21303–21321, 2010

1996), in albedo from optical depths (Oreopoulos and Davies, 1998), in global cloud optical thickness, emissivity and cloud top temperature (Barker et al., 1996; Rossow et al., 2002), and in liquid water path of low-level marine clouds over the Pacific (Wood and Hartmann, 2006). These studies showed that different averaging scales result in apparent biases between instruments, and between instruments and models. This effect is illustrated in Fig. 1. Yet analyses of global cloud variables and climate properties occur typically at far coarser scales. For instance, the global radiative budget of the atmosphere has been studied at $10^{\circ} \times 10^{\circ}$ (e.g. Forster and Gregory, 2006); satellite-based observational studies of the hydrological cycle are found at resolutions of $1^{\circ} \times 1^{\circ}$ (Schlosser and Houser, 2007); studies of the global radiative balance from weather analyses are often at resolutions of $2.5^{\circ} \times 2.5^{\circ}$ (Trenberth et al., 2003); global effects of aerosols on clouds driven by micro-scale interactions are modeled at $5^{\circ} \times 5^{\circ}$ and $2.5^{\circ} \times 2.5^{\circ}$ resolutions (Quaas et al., 2009, and references therein).

This paper compares satellite-based inferences of a set of cloud properties relevant to cloud-climate interactions, and looks for the best fit analytical probability distribution functions (PDFs). The properties are: Cloud Fraction (CF), which modulates the amount of radiation reaching the surface and how much is reflected back into space; cloud liquid water path (LWP), which acts as a powerful barrier of outgoing radiation; and cloud particle effective radius (r_e), which modulates the radiative absorption properties of clouds and the Earth's albedo. LWP is derived from r_e and cloud optical depth, τ, through LWP $\propto \rho_w \tau r_e$, with ρ_w the condensed water density (Platnick et al., 2003). Analytical PDFs fitted here, besides gaussians, have been proposed before: beta for CF (Falls, 1974), Gamma for LWP and τ (Newman et al., 1995; Barker et al., 1996) and log-normal for turbulent processes (Monin and Yaglom, 1975). PDFs are for global CF, r_e and LWP, and means and standard deviations are estimated at resolutions from 5 to 500 km using Collection 5 retrievals from the MODerate resolution Infrared Spectrometer (MODIS) aboard the AQUA spacecraft (King et al., 2006).

We quantify the scale-dependence of statistical moments and compare them to predictions for self-similar homogeneous turbulent flows (Monin and Yaglom, 1975; Frisch,

ACPD
10, 21303–21321, 2010

1995). Quantitative empirical evidence for the turbulent nature of clouds from a space-based perspective goes at least back to Lovejoy (1982), who invoked fractal geometry, and continues to come using multifractal statistics (Lovejoy et al., 2009). To the best of our knowledge, previous studies of satellite observations have used raw (Level-1/radiance) data, and gradients thereof in the case of multifractal analysis, while here we use retrieved (standard Level-2) cloud properties. It is reassuring (Davis et al., 1994) to see that, in spite of all the assumptions used to process radiances into standard cloud products, the signature of turbulence is still clear and can be represented simply enough for practical parameterization of cloud processes in climate models.

2 Analytical PDFs at different scales

Figure 2 shows global PDFs for CF, r_e, and LWP observed over 10 equinox days in 2003 to 2007 at seven spatial resolutions. Equinox days minimize possible seasonal biases while handling the large amount of high spatial resolution data needed to cover a significant number of years. The data are from five-minute granules of MODIS-AQUA daytime observations. A granule covers about $1354 \times 2030\,km^2$ and is treated as if it were a "realization" of a cloud experiment. This resulted in about 2880 realizations. Cloud fraction was considered where CF and Cloud Top Pressure (CTP) were flagged as useable. LWP and r_e are for the same clouds if the LWP is flagged by MODIS as useable. CTP flags were checked to limit the differences in cloud populations from this study to those that discriminate cloud heights. Data confidence levels were allowed to be marginal, good and very good. This assumes that marginal retrievals can return instantaneously incorrect but plausible values. Cloud properties (CF, LWP, r_e, CTP) were extracted for each granule and statistical moments computed within the granule at seven different resolutions: 5, 10, 25, 50, 100, 250, and 500 km. No constraints were set on the percentage of valid retrievals in each scene, their CTP, or if the clouds were over land or ocean. Analytical PDFs were fitted at all spatial resolutions to the observed CF, LWP and r_e distributions using a non-linear least-squares approach with two fitting parameters related to the mean and standard deviation. As expected (Falls,

ACPD
10, 21303–21321, 2010

1974), the observed bimodal PDF of CF is best fit to a beta distribution. The CF is the 5 km resolution MODIS cloud product where the only possible values are 1 and 0 (overcast or clear). As the spatial resolution is degraded, Fig. 2a shows that a continuum of values emerges through averaging clear and overcast scenes onto one mean value. At the coarser resolutions of 250 km and above, the higher peak shifts from 1 towards 0.9. This scale-dependent behavior of CF is consistent with that found for clear scenes using the MODIS 1-km cloud mask (Krijger et al., 2007) where confidence levels (confident cloudy, probably cloudy, probably clear, confident clear) were translated into percentages of clear sky at 1 km and lower spatial resolutions.

Unlike CF, LWP and r_e have a (theoretically) unbounded range of values. Both show skewed, hence non-gaussian, distributions in Fig. 2. Figure 2d–f shows that the log-normal is a better choice for LWP at resolutions finer than 100 km × 100 km, the Gamma function is better at coarser resolutions. The log-normal PDF, a popular choice in turbulence, is a good choice for LWP (Fig. 2b). Gamma PDFs provide the best fit to r_e at all scales (Fig. 2f), which is consistent with how r_e depends on cloud droplet radius (Pointikis and Hicks, 1992) and how droplet radius follows Weibull/Gamma distributions (Liu and Daum, 2002). Figure 2b and c shows that the peak (mode) and tails of LWP and r_e PDFs change with spatial resolution. Large deviations determine the tails on LWP and r_e distributions in these figures. As the spatial resolution is decreased, the averages over larger areas blur these extreme values. As a result, the distributions at coarser resolutions appear more symmetric, the means shift closer to the peaks of the distributions and the tails shorten.

3 Scale dependence of statistical moments

Figure 3 shows the scale dependence of global statistical moments for CF, LWP and r_e calculated by extracting first the average of each variable over spatial domains, that we will call "pixels" of side length L, and then calculating the global average and standard deviation of all those local pixel means. The moments in Fig. 3 all change as a function

ACPD
10, 21303–21321, 2010

of scale. The normalized mean is also shown, it is the inverse of the global "relative dispersion" in Pointikis and Hicks (1992); and the square root of the global "homogeneity parameter" in Wood and Hartmann (2006). The normalized mean enables to compare the relevance of the scale-dependence for variables with different values. Numerical values in Table 1 show mean CF and LWP more scale-dependent than r_e. At the same time, the normalized mean (and the dispersion) for r_e changes over a factor two.

Kostinski and Shaw (2001) argued that cloud particle aggregations at microphysics scales obey statistics similar to those of binary-valued fields with an auto-correlation functions decaying as scale increases. An exponential decay reveals a discrete Poisson distribution of cloudy-clear interfaces. If CF is decorrelated at 5 km (as suggested by results in Schutgens and Roebeling, 2009), then consecutive sampling of CF from uncorrelated pixels is analogous to a temporal sampling of a random binary (cloudy-clear) outcome, time being proportional to the number of pixels sampled. Therefore, if CF statistics follow such Poisson-type rules and self-similarity holds up to 5-km resolution, the absolute deviation would approach the mean value. This is not seen in Fig. 2a where mean CF over its standard deviation decreases with increasing pixel size but remains above unity for all the range 5 to 500 km.

Normalized mean LWP approaches unity at the $100 \times 100\,\mathrm{km}^2$ pixel size, despite LWP not being a bimodal distribution. A possible explanation could come from arguments similar to those from turbulence theory (Frisch, 1995) where the scale-dependence of statistical moments for a variable, X, gives information about how its variance is transferred across scales in turbulent flows. Following Jiménez (2007), we define a generalized structure function of order n as: $S_X(n) = \int X^n P(X)\, dX$, $P(X)$ being its PDF. $S_X(n)$ is used to define a generalized flatness factor as $Y_X(n) = S_X(n)/S_X(2)^{n/2}$. Kolmogorov's self-similarity hypothesis for homogeneous turbulence (X is velocity v) leads to the scaling law $S_v(n) \sim L^{n/3}$, at least for low n, and thus $Y_v(n)$ is independent of L. Note that the normalized LWP means in Fig. 3b are $Y_{\mathrm{LWP}}(1) = \frac{\langle\langle \mathrm{LWP}\rangle\rangle_{\mathrm{global}}}{\langle\langle (\mathrm{LWP})^2 - \langle\langle \mathrm{LWP}\rangle\rangle^2_{\mathrm{global}}\rangle^{1/2}_{\mathrm{global}}}$, overlooking that in turbulence X is a centered (zero-mean) random variable. The

ACPD
10, 21303–21321, 2010

scaling in Fig. 2b for LWP at pixel sizes of $100 \times 100\,\mathrm{km}^2$ and larger is then consistent with that that of self-similar turbulent flows in the inertial subrange.

The observed $Y_{\mathrm{CF}}(1)$ and $Y_{r_e}(1)$ do not converge to unity in Fig. 3a, but approach a linear law in the inverse pixel side length, $1/L$. A linear fit, $\tilde{Y}_{\mathrm{CF}} = 3.03 + 88.21/L$ was found with mean absolute deviation $\Delta_{\mathrm{CF}} = 100 \times \langle |1 - \tilde{Y}_{\mathrm{CF}}(1)/Y_{\mathrm{CF}}| \rangle = 0.9\%$. Similar fits to the global normalized means for LWP and r_e yield $\tilde{Y}_{\mathrm{LWP}} = 1.18 + 10.26/L$ and $\tilde{Y}_{r_e} = 3.25 + 20.17/L$ respectively, with larger mean absolute deviations $\Delta_{\mathrm{LWP}} \approx \Delta_{r_e} = 5.5\%$. As expected from a turbulence perspective, global means change far less than standard deviations when looking for power laws in L. Specifically, we find $\langle \mathrm{CF} \rangle = 0.8L^{0.004}$ ($\Delta = 1\%$), $\langle \mathrm{LWP} \rangle = 124L^{0.013}$ ($\Delta = 1.6\%$), and $\langle r_e \rangle = 19.6L^{-0.001}$ ($\Delta = 0.1\%$), while $\langle \mathrm{CF'}^2 \rangle^{1/2} = 0.06L^{0.24}$ ($\Delta = 5.6\%$) $\langle \mathrm{LWP'}^2 \rangle^{1/2} = 33L^{0.24}$ ($\Delta = 6.6\%$), $\langle r_e'^2 \rangle^{1/2} = 2.3L^{0.18}$ ($\Delta = 6.1\%$), which approach $L^{1/4}$.

4 PDFs of locally normalized means

In essence, Fig. 4 shows statistics of statistics as a function of scale. The PDFs are for means over each pixel normalized locally by the standard deviation over all observations within the pixel. Because CF is given at $5 \times 5\,\mathrm{km}^2$, a minimum of $25 \times 25\,\mathrm{km}^2$ is necessary for the CF pixels to accumulate some significant standard deviation. The notable finding is that, while the global PDFs of CF, LWP, and r_e display different functional forms in Fig. 2, the global PDFs of locally normalized means have a very similar shape for all variables and all are fitted best by log-normal distributions. Notice that the PDFs have been displayed in log-scales making the tails more visible and, as is often seen in turbulence, they appear to be power-law. However, they contribute little to the absolute deviation from the fit when weighted by their frequency of occurrence. Indeed, weighting the absolute deviations by the observed value (thin lines in Fig. 5a–c) measures the deviation from the functional shape, and this shows that the log-normal remains best for LWP and r_e at all domain sizes and it worsens for CF at resolutions finer than $250 \times 250\,\mathrm{km}^2$.

ACPD
10, 21303–21321, 2010

5 Summary and conclusions

Notwithstanding MODIS measurement errors (Boers et al., 2006; Horváth and Davies, 2007; Bennartz, 2007; de la Torre Juárez et al., 2009) and those biases caused by incomplete sampling of highly variable fields (Oreopoulos et al., 2009; Schutgens and Roebeling, 2009), this study has intercompared a set of analytical functions that best fit the observed PDFs of global macroscopic cloud properties across a large range of scales. Observed cloud fraction is best approached by beta distributions, droplet effective radius by a Gamma PDF, and liquid water path follows closely a log-normal or a Gamma distribution. Gaussian PDFs are never the best description.

The global normalized mean CF decreases linearly with the size L of the local averaging domain down to about $100 \times 100\,\mathrm{km}^2$ areas, at which point it trends upward to a resolution of $500 \times 500\,\mathrm{km}^2$. Average LWP changes little from $10 \times 10\,\mathrm{km}^2$ to $100 \times 100\,\mathrm{km}^2$ where it starts increasing linearly with $1/L$. Globally averaged r_e seems to be independent of the spatial resolution. However, normalized means of r_e separate more, with a linear dependence on $1/L$. The mode of the finer resolution CF and the coarser LWP distributions approach unity, which is consistent with the domain-level statistics following self-similar scaling: $Y_\mathrm{LWP}(1) \sim$ constant, as described earlier, in analogy with turbulence theory and observations. Furthermore, when testing for possible connections to self-similar Poissonian statistics, CF fails at 5 km and above.

PDFs of locally normalized mean CF, LWP and r_e (mean over standard deviation inside pixels of a given size) measure the heterogeneity of clouds within each pixel and follow a scale-dependent log-normal distribution for all three variables, thus providing a possible unified description of these cloud properties at all scales in climate model parameterizations of sub-grid processes. Still, the normalized PDFs have tails associated with extreme values and unusually low variability missed by the closest log-normal or Gamma. Normalized CF at resolutions higher than 250 km × 250 km is better approached by a Gamma distribution.

ACPD
10, 21303–21321, 2010

The scale dependence of cloud variability highlights that care is needed to choose a spatial resolution for analyses of global cloud-radiative effects. Rossow et al. (2002) argue that significant horizontal radiative transfer at scales below 3 km justify considering cloud properties at scales only above 3 km for global analyses based on two-stream (up-down) radiative models. This hypothesis may be tested by looking at the radiative impacts of clouds with different sizes and cloud fractions at small scales. Since MODIS CF and τ statistics over $5 \times 5\,km^2$ regions are expected to differ little from the values at 3 km (Dey et al., 2008), 5 km would be a good choice for such a future analysis.

Acknowledgements. Funding provided by the NASA MEaSURES and NEWS programs. The work was carried out at the Jet Propulsion Laboratory/California Institute of Technology, under a contract with the National Aeronautics and Space Administration. Conversations with J. Teixeira and J. Jiménez are gratefully acknowledged. MODIS data are from http://ladsweb.nascom.nasa.gov/., Numpy, Scipy modules and the Generic Mapping Tools were used for this work.

References

Barker, H., Wielicki, B., and Parker, L.: A parameterization for Computing Grid-Averaged Solar Fluxes for Inhomogeneous Marine Boundary Layer Clouds – Part II: Validation using satellite data., J. Atmos. Sci., 53, 2304–2316, 1996. 21306

Bennartz, R.: Global assessment of marine boundary layer cloud droplet number concentration from satellite, J. Geophys. Res., 112, D02201, doi:10.1029/2006JD007547, 2007. 21305, 21311

Boers, R., Acarreta, J. R., and Gras, J. L.: Satellite monitoring of the first indirect aerosol effect: Retrieval of the droplet concentration of water clouds, J. of Geophys. Res., 111, D22208, doi:10.1029/2005JD006838, 2006. 21305, 21311

Budyko, M.: The effect of solar radiation variations on the climate of the Earth, Tellus, 21, 611–619, 1969. 21304

Davis, A., Marshak, A., Wiscombe, W., and Cahalan, R.: Multifractal characterizations of non-stationarity and intermittency in geophysical fields: Observed, retrieved, or simulated, J. Geophys. Res., D99, 8055–8072, 1994. 21307

ACPD

10, 21303–21321, 2010

de la Torre Juárez, M., Kahn, B. H., and Fetzer, E. J.: Cloud-type dependencies of MODIS and AMSR-E liquid water path differences, Atmos. Chem. Phys. Discuss., 9, 3367–3399, doi:10.5194/acpd-9-3367-2009, 2009. 21305, 21311
Dey, S., Girolamo, L. D., and Zhao, G.: Scale effect on statistics of the macrophysical properties of trade wind cumuli over the tropical western Atlantic during RICO, J. Geophys. Res., 113, D24214, doi:10.1029/2008JD010295, 2008. 21305, 21312
Falls, L. W.: The Beta Distribution: A Statistical Model for World Cloud Cover, J. Geophys. Res., 79, 1261–1264, 1974. 21306, 21307
Forster, P. M. F. and Gregory, J. M.: The climate Sensitivity and its components diagnosed from Earth Radiation Budget Data, J. Climate, 19, 39–52, doi:10.1175/JCLI36111, 2006. 21306
Frisch, U.: Turbulence: The Legacy of A. N. Kolmogorov, Cambridge University Press, 1995. 21306, 21309
Hannart, A., Dufresne, J.-L., and Naveau, P.: Why climate sensitivity may not be so unpredictable, Geophys. Res. Lett., 36, L16707, doi:10.1029/2009GL039640, 2009. 21304, 21305
Horváth, A. and Davies, R.: Comparison of microwave and optical cloud water path estimates from TMI, MODIS and MISR, J. Geophys. Res.-Atmos., 112, D01201, doi:10.1029/2006JD007, 2007. 21305, 21311
Imkeller, P. and v. Storch, J.-S. eds.: Stochastic Climate Models, Birkhäuser Verlag, Basel, Schweiz, 2001. 21304
Jiménez, J.: Intermittency in turbulence, in: Proc. 15th “Aha Huliko” a Winter Workshop, Extreme Events, 81–90, 2007. 21309
King, M. D., Platnick, S., Hubanks, P. A., Arnold, G. T., Moody, E. G., Wind, G., and Wind, B.: Collection 005 Change Summary for the MODIS Cloud Optical Property (06_OD) Algorithm, available at: http://modis-atmos.gsfc.nasa.gov/products_C005update.html, (last access: 2009), 2006. 21306
Kostinski, A. and Shaw, R.: Scale-dependent droplet clustering in turbulent clouds, J. Fluid Mech., 434, 389–398, 2001. 21309
Krijger, J. M., van Weele, M., Aben, I., and Frey, R.: Technical Note: The effect of sensor resolution on the number of cloud-free observations from space, Atmos. Chem. Phys., 7, 2881–2891, doi:10.5194/acp-7-2881-2007, 2007. 21308
Liu, Y. and Daum, P.: Indirect warming effect from dispersion forcing, Nature, 419, 580–581, 2002. 21308
Lovejoy, S.: The Area-Perimeter Relation for Rain and Cloud Areas, Science, 216, 185–187,

ACPD
10, 21303–21321, 2010

1982. 21307
Lovejoy, S., Schertzer, D., Allaire, V., Bourgeois, T., King, S., Pinel, J., and Stolle, J.: Atmospheric complexity or scale by scale simplicity?, Geophys. Res. Lett., 36, L01801, doi:10.1029/2008GL035863, 2009. 21307
Monin, A. and Yaglom, A.: Statistical Fluid Mechanics, M.I.T. Press, Cambridge, MA, USA, 1975. 21306
Newman, W., Lew, J., Siscoe, G., and Fovell, R.: Systematic effects of randomness in radiative transfer, J. Atmos. Sci., 52, 427–435, 1995. 21306
Oreopoulos, L. and Davies, R.: Plane Parallel Albedo Biases from Satellite Observations – Part I: Dependence on Resolution and Other Factors, J. Climate, 11, 919–932, 1998. 21306
Oreopoulos, L., Platnick, S., Hong, G., Yang, P., and Cahalan, R. F.: The shortwave radiative forcing bias of liquid and ice clouds from MODIS observations, Atmos. Chem. Phys., 9, 5865–5875, doi:10.5194/acp-9-5865-2009, 2009. 21311
Pierrehumbert, R.: Anomalous scaling of high cloud variability in the tropical Pacific, Geophys. Res. Lett., 23, 1095–1098, 1996. 21305
Platnick, S., King, M., Ackerman, S., Menzel, W., Baum, B., Riedl, C., and Frey, R.: The MODIS cloud products: Algorithms and examples from Terra, IEEE T. Geosci. Remote, Aqua Special Issue, 41, 459–473, 2003. 21306
Pointikis, C. and Hicks, E.: Contribution to the cloud droplet effective radius parameterization, Geophys. Res. Lett., 19, 227–2230, 1992. 21308, 21309
Pujol, T.: Eddy heat diffusivity at maximum dissipation in a radiative-convective one-dimensional climate model, J. Meteorol. Soc. Jpn., 81, 305–315, 2003. 21304
Quaas, J., Ming, Y., Menon, S., Takemura, T., Wang, M., Penner, J. E., Gettelman, A., Lohmann, U., Bellouin, N., Boucher, O., Sayer, A. M., Thomas, G. E., McComiskey, A., Feingold, G., Hoose, C., Kristjánsson, J. E., Liu, X., Balkanski, Y., Donner, L. J., Ginoux, P. A., Stier, P., Grandey, B., Feichter, J., Sednev, I., Bauer, S. E., Koch, D., Grainger, R. G., Kirkevåg, A., Iversen, T., Seland, Ø., Easter, R., Ghan, S. J., Rasch, P. J., Morrison, H., Lamarque, J.-F., Iacono, M. J., Kinne, S., and Schulz, M.: Aerosol indirect effects - general circulation model intercomparison and evaluation with satellite data, Atmos. Chem. Phys., 9, 8697–8717, doi:10.5194/acp-9-8697-2009, 2009. 21306
Roe, G. and Baker, M.: Why Is Climate Sensitivity So Unpredictable?, Science, 318, 629–632, 2007. 21304, 21305
Rossow, W., Delo, C., and Cairns, B.: Implications of the Observed Mesoscale Variations of

ACPD
10, 21303–21321, 2010

Clouds for the Earth's Radiation Budget, J. Climate, 15, 557–585, 2002. 21306, 21312
Schlosser, C. A. and Houser, P. R.: Assessing a Satellite-Era Perspective of the Global Water Cycle, J. Climate, 20, 1316–1338, doi:10.1175/JCLI40571, 2007. 21306
Schutgens, J. and Roebeling, R. A.: Validating the Validation: The Influence of Liquid Water Distribution in Clouds on the Intercomparison of Satellite and Surface Observations, J. Atmos. Ocean. Tech., 26, 1457–1474, 2009. 21305, 21309, 21311
Sellers, W.: A climate model based on the energy balance of the earth-atmosphere systems, J. Appl. Meteorol., 8, 392–400, 1969. 21304
Shenk, W. and Salomonson, V.: A simulation study exploring the effects of sensor spatial resolution on estimates of cloud cover from satellites, J. Appl. Meteorol., 11, 214–220, 1972. 21305
Solomon, S.: Climate Change 2007: The physical science basis., Tech. rep., International Panel on Climate Change, Cambridge, UK, 2007. 21304
Trenberth, K. E., Stepaniak, D. P., and Caron, J.: Accuracy of atmospheric energy budgets, J. Climate, 15, 3343–3360, 2003. 21306
Wood, R. and Hartmann, D. L.: Spatial Variability of Liquid Water Path in Marine Low Cloud: The Importance of Mesoscale Cellular Convection, J. Climate, 19, 1748–1764, doi:10.1175/JCLI37021, 2006. 21306, 21309

ACPD
10, 21303–21321, 2010

Table 1. Observed means, standard deviations and dispersions (inverse of the normalized means) in the panels of Fig. 4. Parentheses show the %-difference of every mean from the mean of all means, i.e., the global average.

Variable	Moment	5 km	10 km	25 km	50 km	100 km	250 km	500 km
	Mean			0.82 (0.8%)	0.81 (−1.1%)	0.80 (−1.4%)	0.82 (0.1%)	0.83 (1.6%)
CF	Standard			0.12	0.17	0.20	0.24	0.26
	Dispersion			0.15	0.21	0.25	0.29	0.32
	Mean	135.28 (−0.7%)	134.20 (−1.5%)	133.00 (−2.4%)	133.18 (−2.3%)	134.79 (−1.1%)	140.38 (3.0%)	143.22 (5.1%)
LWP	Standard	42.8	58.8	78.5	91.5	103.7	122.3	136.2
	Dispersion	0.32	0.44	0.59	0.69	0.77	0.87	0.95
	Mean	19.54 (0.1%)	19.57 (0.1%)	19.57 (0.1%)	19.57 (0.0%)	19.54 (−0.1%)	19.52 (−0.1%)	19.51 (−0.1%)
r_e	Standard	2.75	3.57	4.50	5.08	5.59	6.21	6.70
	Dispersion	0.14	0.18	0.23	0.26	0.29	0.32	0.34

ACPD
10, 21303–21321, 2010

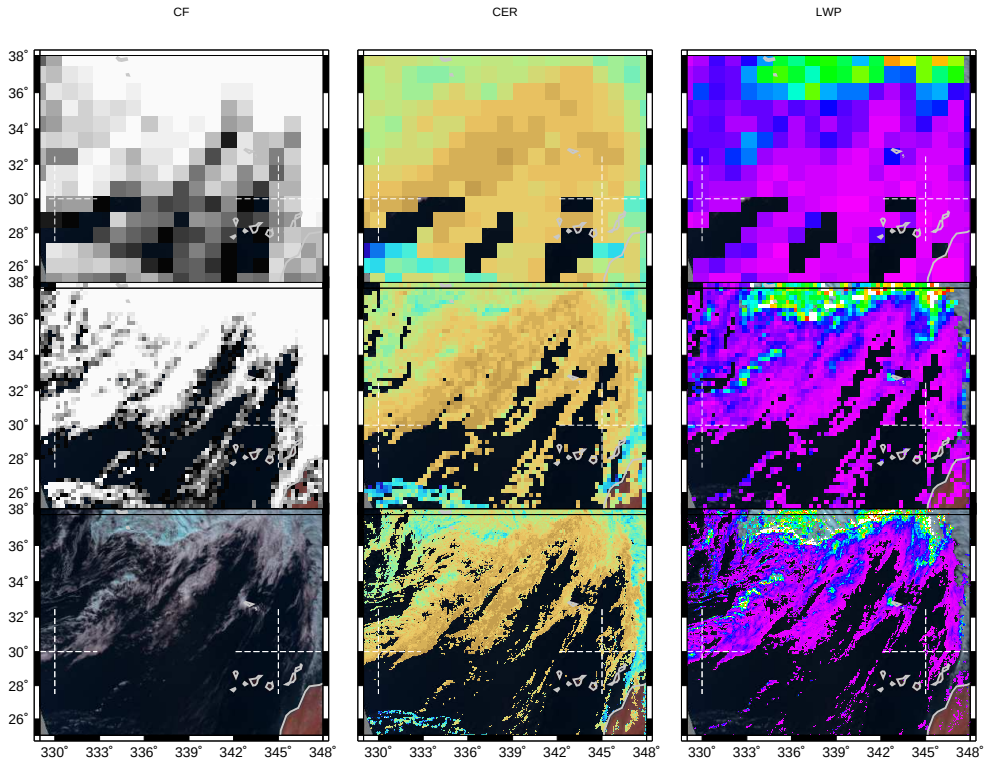

Fig. 1. Cloud fraction (CFR), cloud droplet effective radius (CER) and cloud liquid water path (CLWP) for high and low clouds E and NE of the Canary Islands at spatial resolutions of 5 km, 25 km and 100 km. Different spatial resolutions suggest different statistics of cloud properties. The bottom left scene is a composite of blue-green-IR calibrated radiances from MODIS Band 3 (459–479 nm), Band 4 (545–565 nm), and Band 5 (1230–1250 nm).

ACPD
10, 21303–21321, 2010

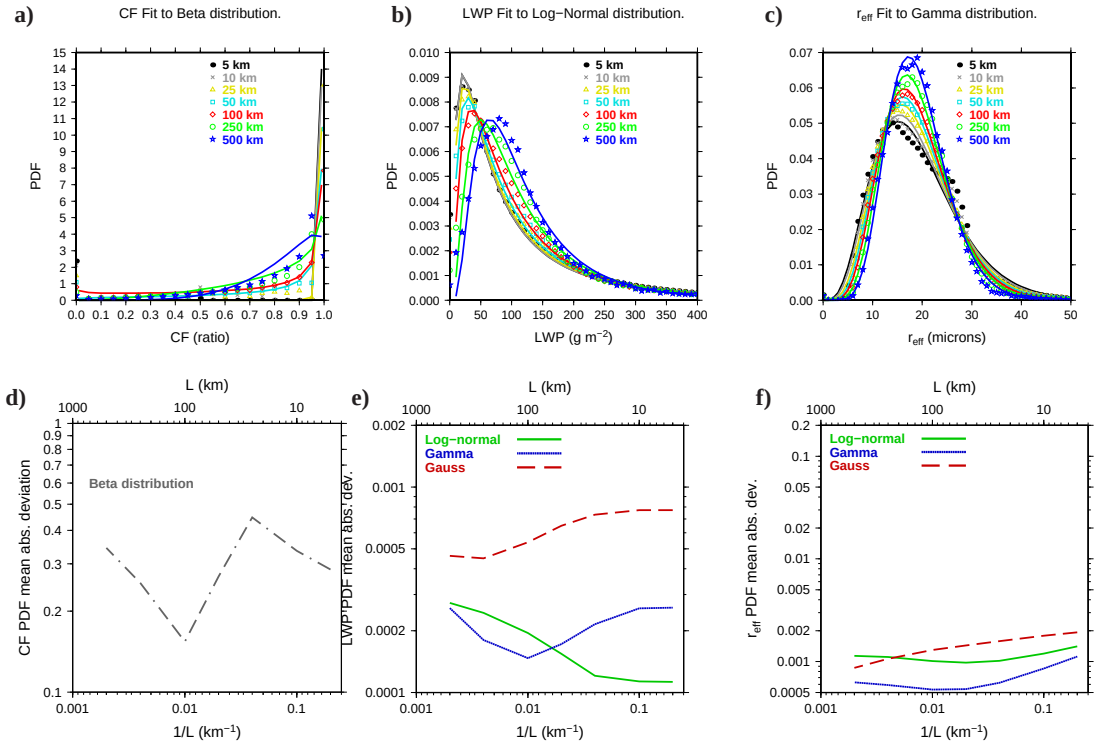

Fig. 2. (a-c) Symbols show the observed values at different spatial averaging scales. Solid lines are the designated least-squares fits. All PDFs for all variables are non-symmetric. LWP and r_e have respectively log-normal and exponential tails that capture the infrequent high values. **(d-f)** Mean absolute deviations between the observed global CF **(d)**, LWP **(e)**, r_{eff} **(f)** and the analytical PDFs after a nonlinear least-squares fit.

ACPD
10, 21303–21321, 2010

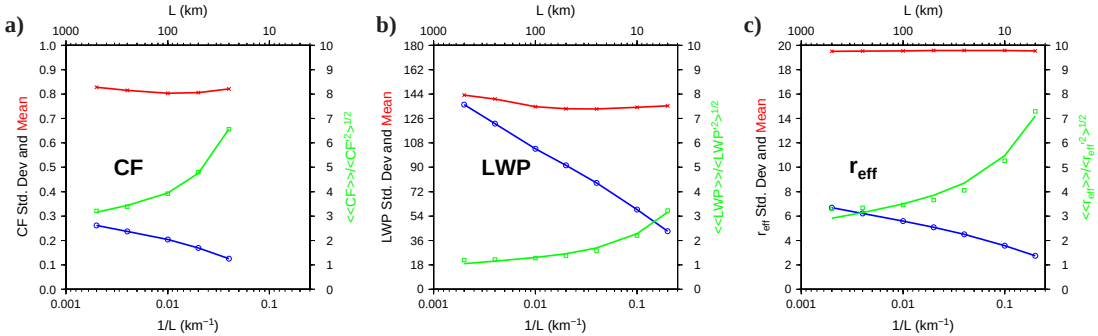

Fig. 3. Scale dependence of the global mean (red), global standard deviations (blue), and mean rescaled over the global standard deviation (green) for CF, LWP and r_e. The double brackets $<<\cdots>>$ stand for "global/ensemble average of local means (at a specific scale)". The primed quantities are deviations from the global average value.

ACPD
10, 21303–21321, 2010

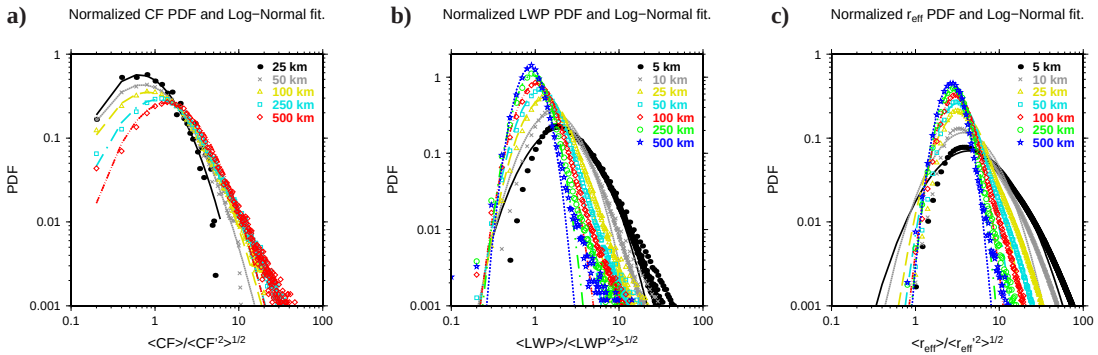

Fig. 4. A different look into cloud property PDFs: means normalized by standard deviations as a function of scale.

ACPD
10, 21303–21321, 2010

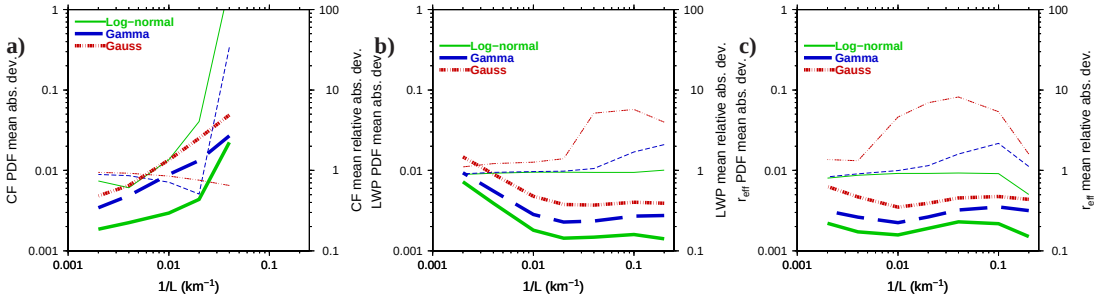

Fig. 5. Mean absolute deviations between the observed and the analytical PDFs in thick lines; thin lines show the mean absolute deviation between fit and observations when weighted by the inverse of the observed PDF at each point.

ACPD
10, 21303–21321, 2010